PLOS ONE

RESEARCH ARTICLE

Atherosclerosis is associated with a decrease in cerebral microvascular blood flow and tissue oxygenation

Baoqiang Li[1,2☯], **Xuecong Lu**[1,2☯], **Mohammad Moeini**[3], **Sava Sakadžić**[4], **Eric Thorin**[2,5], **Frederic Lesage**[1,2*]

1 Institute of Biomedical Engineering, École Polytechnique de Montréal, Montréal, QC, Canada, **2** Research Center, Montreal Heart Institute, Montréal, QC, Canada, **3** Department of Biomedical Engineering, Amirkabir University of Technology (Tehran Polytechnic), Tehran, Iran, **4** Athinoula A. Martinos Center for Biomedical Imaging, Massachusetts General Hospital, Harvard Medical School, Charlestown, MA, United States of America, **5** Department of Surgery, Faculty of Medicine, University of Montreal, Montréal, QC, Canada

☯ These authors contributed equally to this work.
* frederic.lesage@polymtl.ca

Citation: Li B, Lu X, Moeini M, Sakadžić S, Thorin E, Lesage F (2019) Atherosclerosis is associated with a decrease in cerebral microvascular blood flow and tissue oxygenation. PLoS ONE 14(8): e0221547. https://doi.org/10.1371/journal.pone.0221547

Editor: Johannes Boltze, University of Warwick, UNITED KINGDOM

Received: November 30, 2018

Accepted: August 11, 2019

Published: August 30, 2019

Data Availability Statement: All relevant data are included within the paper and its Supporting Information files.

Funding: This study was supported with a discovery grant from the Natural Sciences and Engineering Research Council of Canada awarded to F.L. The funders had no role in study design, data collection and analysis, decision to publish, or preparation of the manuscript.

Competing interests: The authors have declared that no competing interests exist.

Abstract

Chronic atherosclerosis may cause cerebral hypoperfusion and inadequate brain oxygenation, contributing to the progression of cognitive decline. In this study, we exploited two-photon phosphorescence lifetime microscopy to measure the absolute partial pressure of oxygen (PO_2) in cortical tissue in both young and old $LDLR^{-/-}$, $hApoB100^{+/+}$ mice, spontaneously developing atherosclerosis with age. Capillary red-blood-cell (RBC) speed, flux, hematocrit and capillary diameter were also measured by two-photon imaging of FITC-labelled blood plasma. Our results show positive correlations between RBC speed, flux, diameter and capillary-adjacent tissue PO_2. When compared to the young mice, we observed lower tissue PO_2, lower RBC speed and flux, and smaller capillary diameter in the old atherosclerotic mice. The old mice also exhibited a higher spatial heterogeneity of tissue PO_2, and RBC speed and flux, suggesting a less efficient oxygen extraction.

Introduction

Chronic atherosclerosis has a lifelong impact on brain health [1–9]. It can cause cerebral hypoperfusion and cerebrovascular disorders [10–12], which, in turn, impairs normal cognitive function [12–15]. Reduced supply of oxygen to brain tissue due to the atherosclerosis-related disruption in cerebral blood flow may induce neurodegeneration [16,17], leading to cognitive decline. The cerebral capillary network is the major site of vessel-tissue oxygen exchange [18]. The role of capillaries in oxygen delivery was emphasized in several modeling studies showing that brain tissue oxygenation benefits from not only the increase in absolute capillary blood flow but also from its homogenization [19–21]. Therefore, alterations of brain tissue oxygenation, and capillary structural and functional properties can indicate deviations from normal brain condition.

Little is known, however, about the distribution and change in brain tissue oxygenation, and capillary blood flow with the progression of atherosclerosis. Furthermore, limited experimental data has been published demonstrating how capillary blood flow and flow spatial patterns modulate oxygen extraction. The recent synthesis of an oxygen-sensitive phosphorescence probe PtP-C343, which can be combined with two-photon phosphorescence lifetime microscopy, enabled measurements of the absolute partial pressure of oxygen (PO_2) in the parenchymal tissue of brain at the micron scale [22–24]. Exploiting this key development, we aim here to experimentally characterize the distribution of brain tissue oxygenation and cortical capillary blood flow, as well as to investigate the relation between capillary blood flow homogenization and brain tissue oxygenation, in a mouse model of atherosclerosis.

Based on two-photon lifetime imaging of the phosphorescence from the probe PtP-C343 [22,23], we measured absolute partial pressure of oxygen (PO_2) in the cortical tissue of young and old dislipidemic $LDLR^{-/-}$ mice [25–28]. Capillary red blood cell (RBC) speed, flux, hematocrit and diameter were also measured by two-photon imaging of FITC-labelled blood plasma. We first investigated whether there were correlations between the capillary structural/flow properties and adjacent brain tissue oxygenation in young mice with limited pathology. Performing the same measures in an older group, we then studied age-related differences in cortical tissue PO_2, capillary RBC speed and flux, the degree of capillary blood flow heterogeneity, and capillary diameter.

Materials and methods

Experimental setup

Experiments were conducted with a home-built two-photon laser scanning microscope (Fig 1A). The system details have been described in previous publications [29,30]. Briefly, we employed a laser (80 MHz, 150-fs pulse width, Mai-Tai, Newport) as a two-photon excitation source. The laser power and gating were controlled by an electro-optic modulator (EOM). The laser beam was raster-scanned by a pair of galvanometric scanners. After the galvo mirrors, the laser beam was magnified by a telescope, consisting of a scan lens and a tube lens, and then imaged on the back-aperture of an objective lens (20×, NA = 1.0, water immersed, XLUMPLFLN 20XW, Olympus). Finally, the beam was focused onto the sample for imaging. The emitted photons were filtered by a dichroic mirror (FF685-DI02-25×36, Semrock) and a band-pass filter (FF02-809/81-25, Semrock), and detected by a photomultiplier tubes (PMTs). Phosphorescence from the PtP-C343 probe was detected by one PMT (H7422, Hamamatsu). Fluorescence from a FITC-labeled blood plasma was detected by another PMT (R3896, Hamamatsu). Acquisition was controlled by a home-developed MATLAB-based software.

Animal preparation

In this study, n = 6 young (3–4 months, male, 21–28 g) and n = 6 old (15–20 months, male, 35–45 g) transgenic mice from our established colony were used. This transgenic model (wild-type strain: hybrid of 129SvyEv and C57BLy6) has a deletion of the LDL receptor gene and overexpresses human apo-lipoprotein B ($LDLR^{-/-}$; $hApoB100^{+/+}$). Mice lacking the LDL receptor develop atherosclerosis spontaneously without the need of high cholesterol diet [25,26]. The mouse colony has been established for the last 15 years at the Montreal Heart Institute and with these mice consistent levels of atherogenesis have been reported through the years [27,28,31–35]. In the previous studies with this model, it was shown that the atherosclerotic plaque was not significantly developed in the 3-month-old atherosclerotic mice but that plaque area increased significantly in the atherosclerotic mice starting from 6 months [28,33,34]. Learning ability, evaluated with the Morris water maze test, was preserved in the 3-month-old

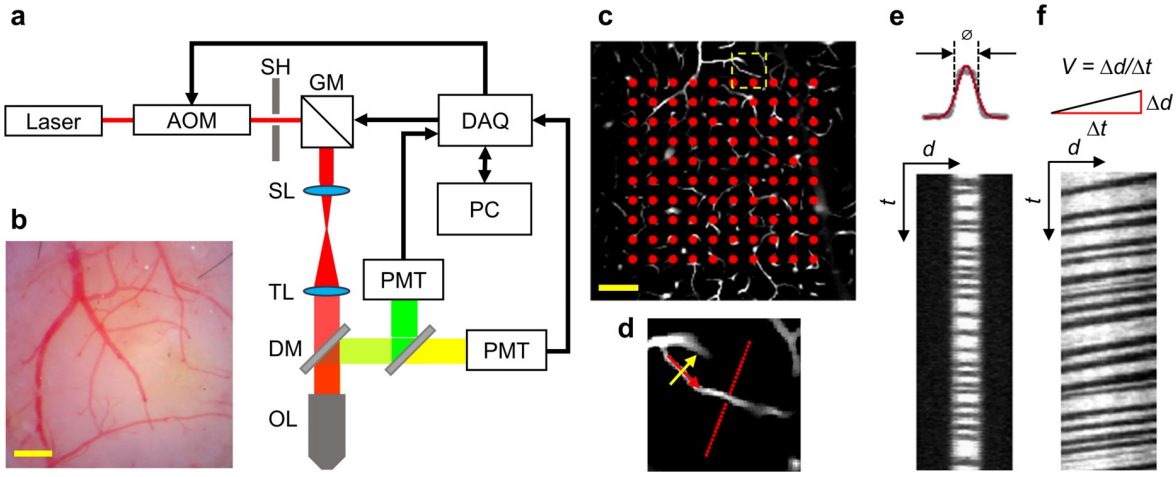

Fig 1. Experimental setup and acquisition protocol. a. Schematic diagram of the two-photon microscopy system. The components are abbreviated as: acousto-optic modulator (AOM), shutter (SH), Galvo mirror (GM), scan lens (SL), tube lens (TL), dichroic mirror (DM), objective lens (OL), photomultiplier tube (PMT), data acquisition card (DAQ), and personal computer (PC). **b.** A representative CCD image capturing the mouse brain surface vasculature. Scale bar: 500 μm. **c.** Illustration of the 2D grid of locations (red dots) marked for PO_2 acquisition performed in the cortical tissue within the capillary bed. The red dashed square encloses a capillary, used as an example of blood flow and tissue PO_2 gradient acquisition in **d**. Scale bar: 50 μm. **d.** The red dots in the vascular image illustrate the measurement locations for tissue PO_2 gradient, perpendicular to the capillary axis. In the same capillary, perpendicular and longitudinal line-scans were performed, as illustrated by the yellow and red arrows, respectively. The arrows indicate the line-scan directions. **e** and **f.** Representative perpendicular (**e**) and longitudinal (**f**) line-scan images utilized to extract capillary RBC flow properties and diameter. In **e**, ø, d and t represent diameter, distance and time, respectively. In **f**, the RBC speed V was calculated by the ratio of the distance interval (Δd) to the time interval (Δt).

https://doi.org/10.1371/journal.pone.0221547.g001

mice, but declined significantly starting from 6-month old, as compared to their age-matched controls [28].

For experiments, mice were first tracheotomised to facilitate animal respiration. Following tracheotomy, a femoral artery cannulation was performed to measure arterial blood gases. Then, an open-skull craniotomy (3 mm in diameter) was done over the primary somatosensory area in the left hemisphere. After the craniotomy, a solution of PtP-C343 (0.6–1.2 μL at 150 μM) was microinjected into brain tissue at 200 μm depth below the brain surface. The cranial window was then filled with agarose diluted in artificial CSF, sealed using a 5-mm diameter microscope coverslip, and the animal was transferred to the two-photon microscope for imaging. Dextran-conjugated FITC (100–200 μL at 50 mg/mL, FD2000S Sigma) was then administered intravenously to visualize micro-vessels enabling localization of the capillary bed for PO_2 imaging and to measure capillary RBC flow properties. The animals were anesthetized by intraperitoneal administration of urethane (1–1.5 g/kg at 10% W/V) throughout all surgical and experimental procedures. Anesthesia was confirmed by the loss of withdrawal response to toe pinch, and could last for ≥4 hours, long enough for performing both surgery and imaging experiment. During all the surgical procedures and imaging, mice were spontaneously breathing an air/oxygen mixture (air mixed with 10–20% oxygen). The mice were euthanized after experiments using CO_2 inhalation. All the surgical and experimental procedures were performed in accordance with the Canadian Council on Animal Care recommendations, and were approved by the animal ethics committee of the Montreal Heart Institute research center (Protocol No: 2013–1619).

Prior to imaging, arterial blood gases were measured by a commercial blood gas analyzer to insure physiological levels. In the young group, arterial partial pressure of oxygen (P_aO_2) was 102.3±1.4 mmHg; arterial partial pressure of carbon dioxide (P_aCO_2) was 37.7±3.2 mmHg; and arterial oxygen saturation (SO_2) was 97.5±0.3%. In the old group, P_aO_2 was 122.0±3.5

mmHg; P_aCO_2 was 40.2±3.0 mmHg; and SO_2 was 98.0±0.6%. Body temperature was maintained at ~37˚C in all mice throughout all experiments. Data are expressed as mean±SEM.

Data acquisition

Tissue PO_2 imaging. A CCD image of the mouse brain surface vasculature was recorded to guide the selection of a region of interest (ROI) for subsequent two-photon imaging (Fig 1B). PO_2 measurements were collected typically at two depths, spanning from 150 μm to 250 μm below the brain surface. At each imaging depth, we first performed a raster-scan of FITC intensity, which revealed the location of the capillaries within a 400 × 400 μm^2 field of view (FOV). Two sets of tissue PO_2 measurements were collected. First, PO_2 measurements were performed in a 2D grid geometry (e.g., 10 × 10 measurement locations as denoted by red dots in Fig 1C) in the parenchymal tissue of the cortical capillary bed. Second, PO_2 was measured in tissue as a function of distance from the capillary wall in the direction perpendicular to the longitudinal axis of the capillary, with sub-micron steps, over a radial distance of 30 μm (Fig 1D).

At each measurement location, the phosphorescent nanoprobe (PtP-C343) in the focal volume was excited with a 25-μs-long laser excitation at 820 nm gated by the EOM, followed by a 275-μs-long collection of the emitted phosphorescence. Typically, at each location, 3,000 such 300-μs-long excitation/decay cycles were repeated to obtain an average phosphorescence decay with sufficient signal-to-noise ratio (SNR) for accurate lifetime calculation. Further technical details have been described in [23,29].

Imaging of capillary RBC flow. In the same capillaries for which PO_2 gradients were measured in the adjacent tissue, RBC speed, flux and hematocrit were measured by performing longitudinal and perpendicular line-scans (Fig 1E and 1F) [36,37] on the FITC-labelled capillaries. The line-scan sampling frequency was 800 Hz, fast enough to accurately measure RBC speed and flux in most cortical capillaries in mice without aliasing effect [38]. The line-scans and tissue PO_2 gradients were acquired sequentially in time, capillary by capillary. The combined acquisitions for each capillary were completed within ≤10 seconds.

Data analysis

Calculation of PO_2. The phosphorescence lifetime was calculated by fitting the average 275-μs phosphorescence decay to a single exponential decay function, using a non-linear least square minimization algorithm [22,23,29]. The lifetime was then converted to absolute PO_2 using a Stern-Volmer type calibration plot obtained in an independent oxygen titration experiment.

Capillary PO2 gradient and wall PO_2. To observe the capillary PO_2 gradient, the PO_2 values were binned with 5-μm bins (Fig 2A). Capillary wall PO_2 was calculated based on tissue PO_2 measured radially in respect to the capillary axis, by averaging the PO_2 values within the first 10 μm from the capillary wall.

Calculation of capillary RBC flow properties and diameter. RBC flux was calculated by counting the number of the dark shadows in the perpendicular (Fig 1E) or longitudinal (Fig 1F) line-scan images during the acquisition time (t). The angle of the dark streaks in the longitudinal line-scan image (Fig 1F) was estimated to calculate the RBC speed as $\Delta d/\Delta t$, where Δd and Δt are the distance and time intervals, respectively. RBC hematocrit was computed as the ratio (in %) of the number of pixels in the dark shadows to the total number of pixels in the longitudinal line-scan image. Capillary diameter was calculated as the full width at half maximum, by fitting the intensity profile along the distance axes (d) of the perpendicular line-scan image with a Gaussian model (Fig 1E). More details about the line-scan acquisition parameters can be found in [29].

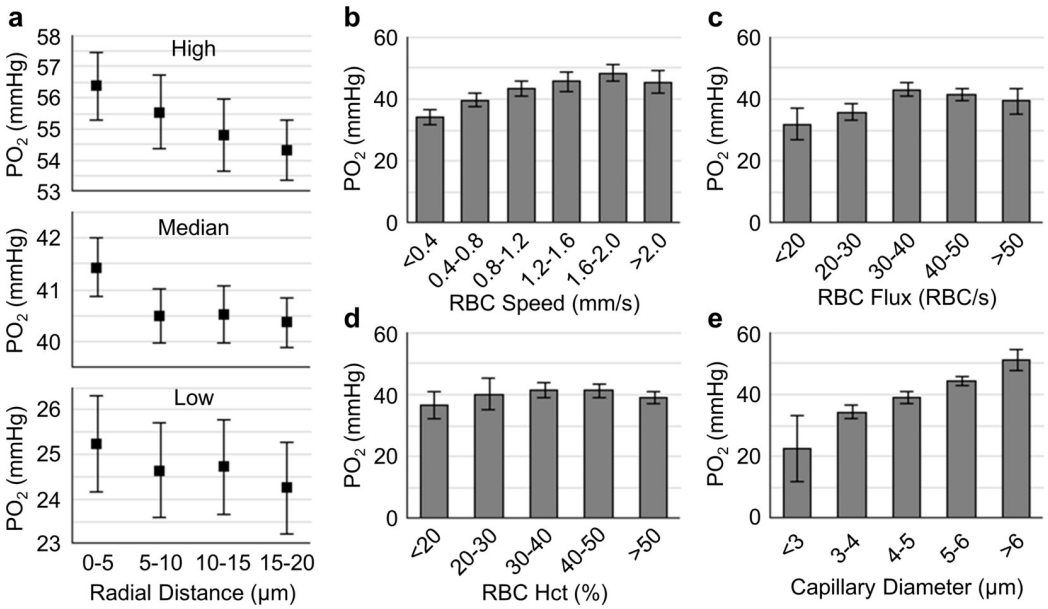

Fig 2. Relations between capillary RBC flow properties, diameters, wall PO_2, and adjacent tissue PO_2 gradients. a. Average tissue PO_2 gradients from high, medium and low wall PO_2 capillary groups, collected across n = 12 mice. **b**-**e.** Relations between RBC speed, flux, hematocrit (Hct), diameter and wall PO_2. The analysis in **b**-**e** was made with the measurements acquired in ~15 capillaries per mouse across n = 12 mice (including both the young and old mice). Data are expressed as mean±SEM.

https://doi.org/10.1371/journal.pone.0221547.g002

Calculation of RBC flow and tissue PO_2 heterogeneity. For each of the measured parameters, its heterogeneity was quantified as standard deviation (STD) and coefficient of variation (CV) of its data population. Here, CV was calculated as the ratio of STD to mean [39].

Statistical analysis. Data are presented as mean±SEM. The measurements in Figs 2–4 were first averaged over capillaries within each mouse, and then across mice. Statistical comparisons in Fig 4 were made using Student's t-Test (MATLAB, MathWorks Inc.). P value less than 0.05 was considered statistically significant. Detailed measurement information is indicated in the text and figure legends, where relevant.

Results

Cortical capillary RBC flow and diameter positively correlate with oxygenation in adjacent tissue

We employed a home-built two-photon laser-scanning microscope (Fig 1A) to measure the resting PO_2 in the parenchymal tissue of the somatosensory cortex of urethane-anesthetized young and old atherosclerotic mice. PO_2 imaging with a 2D grid acquisition geometry (Fig 1C) was performed within a 400 × 400 μm^2 FOV, typically at two depths per mouse from 150 μm to 250 μm below the brain surface. At each imaging depth, PO_2 gradients (Fig 1D) were also acquired in tissue adjacent to capillaries to estimate the capillary wall PO_2. In the same capillaries, whose wall PO_2's were estimated, RBC flux, speed, hematocrit and capillary diameter were measured with the perpendicular and longitudinal line-scan techniques (Fig 1E and 1F) [29,37]. See the METHODS section for details about the experiments, data acquisition and analysis.

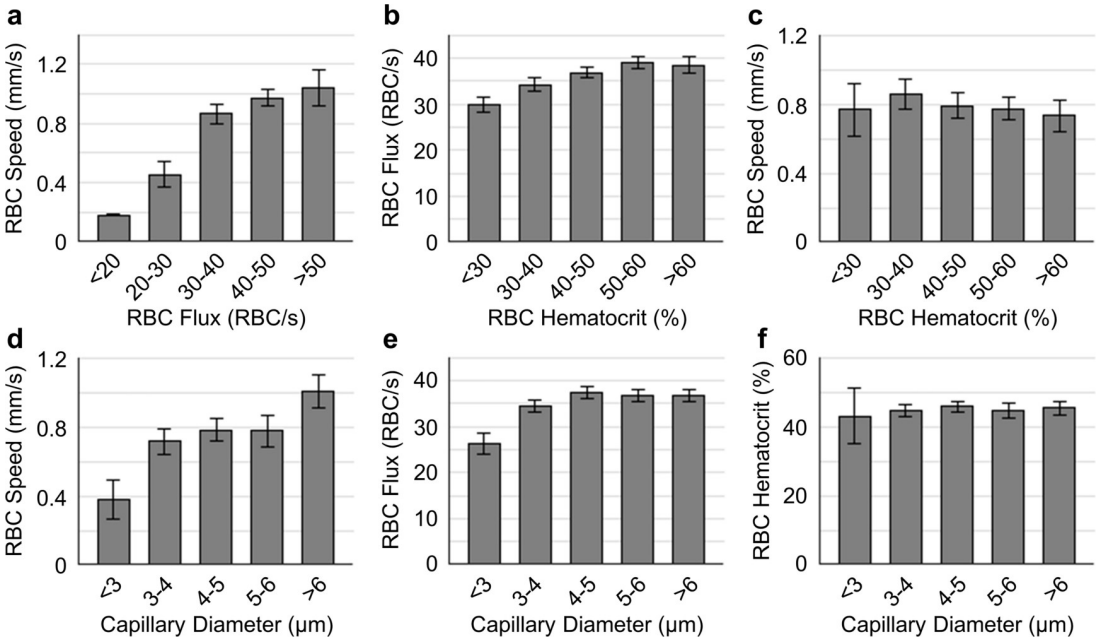

Fig 3. Pairwise relations between capillary RBC flow properties and diameters. a-f. Pairwise relations between RBC speed, flux, Hct and diameter. The analysis in **a-f** was made with the measurements acquired in ~15 capillaries per mouse, across n = 12 mice (including both the young and old mice). Data are expressed as mean±SEM.

https://doi.org/10.1371/journal.pone.0221547.g003

We first investigated the PO_2 changes as a function of radial distance from the capillary wall, perpendicular to the capillary axis. The tissue PO_2 gradients were grouped into three groups having an equal number of capillaries, based on the wall PO_2 values of the associated capillaries: high (>46 mmHg), median (35–45 mmHg) and low (<35 mmHg). The average PO_2 gradient in the high wall PO_2 group exhibited greatest PO_2 decrease with distance from the capillary wall (ΔPO_2 = 2.2 mmHg between PO_2 at 0–5 μm and 15–20 μm from the wall), while such decreasing trend in the median and low wall PO_2 groups was much smaller (~1 mmHg; Fig 1A).

We next investigated the relations between capillary RBC flow properties, diameter and wall PO_2. We observed a positive correlation between RBC speed and wall PO_2 up to speed values of 1.6–2.0 mm/s. The capillary wall PO_2 reached a plateau at higher speeds (Fig 2B). A similar trend was observed between RBC flux and wall PO_2 (Fig 2C), but no clear correlation between RBC hematocrit and wall PO_2 was observed (Fig 2D). Capillary diameter exhibited a strong positive correlation with wall PO_2 (Fig 2E). Linear regressions were carried out on the data to quantify the correlations. The slopes of the correlations between RBC speed, flux, diameter, and wall PO_2 (corresponding to the panels **b, c** and **e**) were calculated to be 8.6 mmHg·s/mm, 0.2 mmHg·s/RBC and 4.7 mmHg/μm, respectively; and the associated coefficients of determination (R^2) were 0.08, 0.02 and 0.11, respectively.

Furthermore, RBC flux exhibited strong positive correlation with speed (Fig 3A). A similar trend was observed in RBC flux vs. hematocrit (Fig 3B). RBC hematocrit was found weakly negatively correlated with speed (Fig 3C). In addition, both RBC flux and speed increased with capillary diameter (Fig 3D and 3E). No clear trend was observed between RBC hematocrit and capillary diameter (Fig 3F). Linear regressions were carried out on the data populations to quantify the correlations. The slopes of the correlations corresponding to panels **a-e** are 0.03 mm/RBC, 20.06 RBC/s, -0.21 mm/s, 0.09 mm/s/μm and 0.64 RBC/s/μm; and the R^2 values are 0.26, 0.08, 0.01, 0.04 and 0.01, respectively.

Cortical tissue PO_2 and capillary RBC flow were lower and more heterogeneous in the older atherosclerotic mice

The absolute values, STD and CV of tissue PO_2, capillary RBC speed, flux, hematocrit and diameter were compared between the young and old atherosclerotic mice. PO_2 gradients adjacent to capillaries and tissue PO_2 measurements were also collected using a 2D grid acquisition geometry in the cortical parenchymal tissue adjacent to the capillary bed. The histograms of tissue PO_2 (combining the PO_2 gradient and 2D-grid PO_2 measurements) acquired in the young and old atherosclerotic mice are presented in S1 Fig.

Absolute tissue PO_2 in the old atherosclerotic mice (39.4±7.0 mmHg) was lower (P = 0.22) than in the young atherosclerotic mice (49.9±4.0 mmHg; Fig 4A). PO_2 STD and CV in the old atherosclerotic mice were noticeably higher than in the young atherosclerotic mice (Fig 4B and 4C).

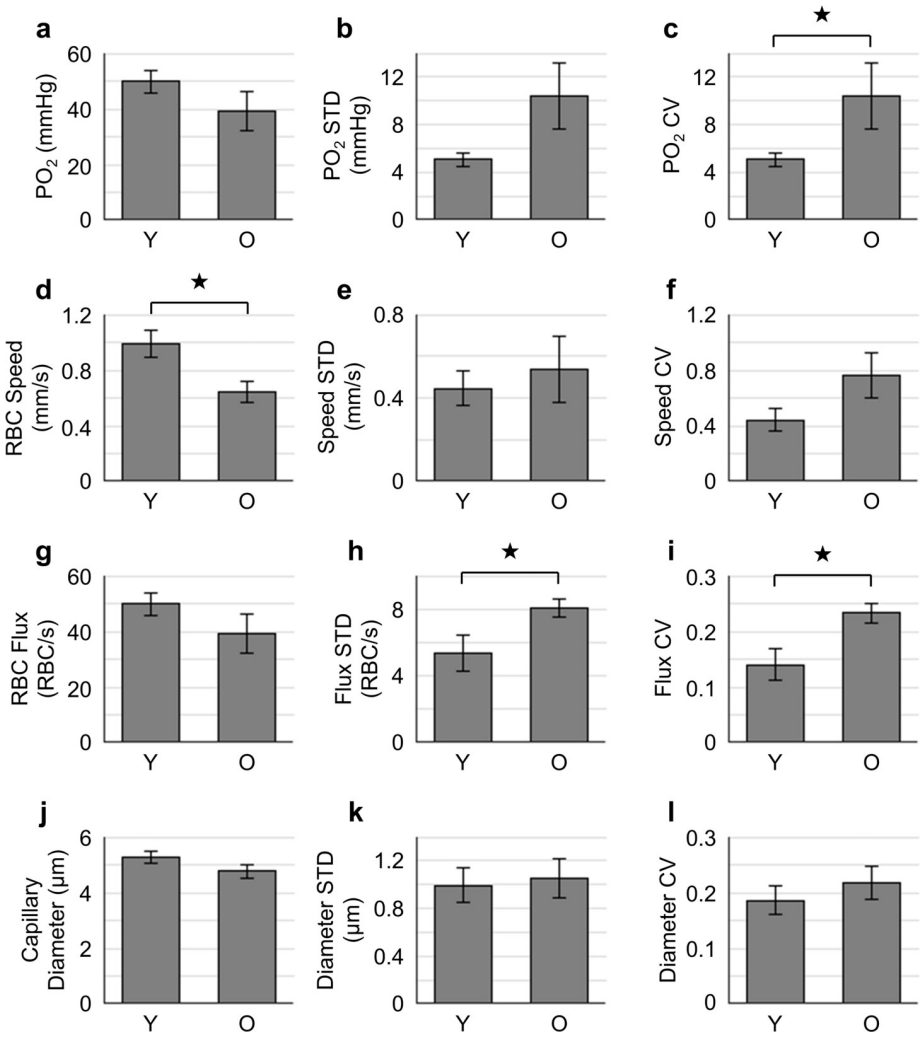

Fig 4. Comparisons of cortical tissue PO_2, capillary RBC flow and diameter between the young (Y) and old (O) atherosclerotic mice. a-c. Absolute tissue PO_2, PO_2 STD and CV; **d-f.** absolute RBC speed, speed STD and CV; **g-i.** absolute RBC flux, flux STD and CV; **j-l.** absolute capillary diameter, diameter STD and CV. The data presented in **a-c** was based on 100–200 samples acquired per mouse. The analysis in **d-l** was made with the measurements acquired in 15 capillaries per mouse. In **a-l**, for each age group, data were first averaged with all the measurements in each mouse, and then over mice. Data are expressed as mean±SEM. The star symbol indicates significant difference ($P<0.05$, Student's t-test).

https://doi.org/10.1371/journal.pone.0221547.g004

Similar changes from old to young were observed in the capillary RBC flow properties. Specifically, absolute RBC speed in the old atherosclerotic mice (0.66±0.08 mm/s) was significantly lower than in the young atherosclerotic mice (0.99±0.10 mm/s; Fig 4D). RBC flux in the old atherosclerotic mice (35.1±1.3 RBC/s) was lower than in the young atherosclerotic mice (39.4±2.1 RBC/s), but did not reach statistical significance (Fig 4G). Both RBC Flux STD and CV were significantly higher in the old atherosclerotic mice than in the young atherosclerotic mice (Fig 4H and 4I). Capillary diameters (Fig 4J) were not significantly different between the two groups despite exhibiting a lower trend in the older mice (Y: 5.3±0.2 μm; O: 4.8±0.2 μm, P = 0.12). No obvious difference was found in RBC hematocrit, and its STD and CV (S2 Fig).

Discussion

It has been reported that chronic atherosclerosis could cause cerebral hypoperfusion and cerebrovascular disorders [10–12], leading to cognitive impairment [12–15]. In this study we measured PO_2 in the cortical tissue of a mouse model of atherosclerosis. Mice lacking the LDL receptor develop atherosclerosis spontaneously, after the age of 3 months, without the need of high cholesterol diet [25,26]. The PO_2 measurements were performed both densely in cortical tissue adjacent to capillaries and over wider areas containing the capillary bed. Capillary RBC speed, flux, hematocrit and diameter were also measured by two-photon imaging of FITC-labelled blood plasma. We analyzed the pairwise relations between tissue PO_2, and capillary RBC flow properties and diameter. We also performed group comparisons to explore the impact of chronic atherosclerosis on brain oxygenation and capillary RBC flow.

We first characterized the tissue PO_2 gradient driven by the oxygen diffusion from capillaries (Fig 2A). Tissue PO_2 gradients around capillaries have been theoretically predicted [40], but not experimental confirmed. We found that around capillaries associated with high wall PO_2, the gradient was higher when compared to those associated with medium and low wall PO_2. There is possibility that the capillaries with high wall PO_2 were topologically and/or physically closer to pre-capillary arterioles in the network, and had higher oxygenation than the capillaries having medium and low wall PO_2, thus contributing more to brain tissue oxygenation [41]. Next, we focused on the relations between capillary wall PO_2 and RBC flow and diameter. It has been reported that tissue PO_2 in proximity to the capillary wall could represent, to some extent, the intra-capillary PO_2 [42]. Our results in Fig 2 show that higher capillary RBC flux results in a greater oxygenation in the adjacent tissue. This result could be inferred from a previous study, in which a positive relation between capillary RBC flux and intra-capillary PO_2 was reported [43]. Furthermore, we analyzed the relations between capillary RBC flow parameters and diameter (Fig 3). Our results showed that both RBC speed and hematocrit were positively related with flux, but hematocrit was slightly negatively related with RBC speed, in agreement with the previous studies [37,43]. In addition, RBC speed and flux increased with capillary diameter, but hematocrit had no clear relation to diameter. Similar results have been reported in previous studies in anesthetized rats [37,44] and mice [36,45].

Absolute tissue PO_2 measured in the capillary bed tended to be lower in the old atherosclerotic mice (Fig 3), although a significant difference was not reached. However, reduced capillary RBC speed, flux and diameter were observed in the old atherosclerotic mice, which differs from previous studies reporting increased RBC speed and flux, and larger capillary diameter in aged mice [29] and rats [44]. Atherosclerosis is associated with vascular endothelial damage [46,47] and cerebral hypoperfusion [11,12] which could decrease capillary diameter thereby limiting RBC flow.

The reduced capillary RBC flow and diameter in the old atherosclerotic mice was accompanied by an increase in the spatial heterogeneity of the same variables (quantified by STD and

CV, Fig 4), implying a compromised oxygen delivery to tissue as predicted by the biophysical models [19,20]. Capillary flow pattern disturbances are not unique to this mouse model of atherosclerosis, but were also found to be involved in the progression of neurodegeneration [21]. It was reported that capillary flow heterogeneity could play a crucial role in focal ischemic stroke, as it could induce local hypoxia and neuronal death, without a detectable decrease in the absolute global cerebral blood flow [48].

The origin of capillary RBC flow heterogeneity remains difficult to identify. We have found smaller average capillary diameter but larger diameter heterogeneity in the old atherosclerotic mice. As capillary RBC flow was reported to be correlated positively with diameter and intravascular PO_2 [43,44], our findings about diameters are in good agreement with the findings about capillary RBC flow and tissue PO_2 (Figs 2 and 3). Therefore, these results imply that a disturbed flow pattern might essentially originate from microvascular structural changes [49].

Limitations exist in this study. Although the animal physiology was carefully controlled in experiments, anesthesia inevitably introduce hemodynamic changes relative to the awake state [50], thus adding variability to the measurements. Furthermore, we cannot exclude the possibility of an anesthetic effect with age which remains a limitation of this study. Nonetheless, in our previous studies in either anesthetized [44] or awake wild-type animals [29], comparisons of the absolute capillary blood flow and flow heterogeneity between the young and old mice followed similar trends, implying that anesthesia may not differentially affect the brain physiology among different age groups. Measurements in age-matched wild-type mice were not available in this study. In the previous work with the same atherosclerotic model, difference in cerebral blood flow between the 3-month and 6–12 month mice was found significantly different [28], but the aging effect on cerebral blood flow, oxygenation and capillary blood flow properties in the healthy wild-type mice occurred much later (e.g., 2-year old) [29].

To conclude, our study for the first time demonstrated that tissue PO_2 was positively correlated with capillary RBC flow and capillary diameter. In addition, we found lower tissue PO_2, lower capillary RBC flow and smaller capillary diameter in the old atherosclerotic mice when compared to younger mice. We also found more spatially heterogeneous distributions of tissue PO_2, RBC flow properties and capillary diameter in the old atherosclerotic mice when compared to the younger mice. Overall, our results confirm a detrimental impact of atherosclerosis on brain oxygenation and microvascular function.

Supporting information

S1 Fig. Histograms of tissue PO_2 measured in the young (Y) and old (O) atherosclerotic mice. The tissue PO_2 distribution in the old atherosclerotic mice is broader and shifted towards the lower PO_2 values when compared to the young mice.
(TIF)

S2 Fig. Comparison of capillary RBC hematocrit (Hct) between the young (Y) and old (O) atherosclerotic mice. a-c. Comparisons of absolute Hct, Hct STD and CV, respectively. The analysis was made with the measurements acquired in 15 capillaries per mouse. The data were first averaged with all the measurements in each mouse, and then over mice. Data are expressed as mean±SEM. No significant difference was found (Student's t-test).
(TIF)

Acknowledgments

The authors thank Marc-Antoine Gillis and Natacha Duquette for their help with the animal preparations. This study was supported with a discovery grant from the Natural Sciences and Engineering Research Council of Canada awarded to Frederic Lesage.

Author Contributions

Conceptualization: Baoqiang Li, Xuecong Lu, Mohammad Moeini, Eric Thorin, Frederic Lesage.

Formal analysis: Baoqiang Li, Xuecong Lu.

Funding acquisition: Frederic Lesage.

Investigation: Baoqiang Li, Xuecong Lu, Frederic Lesage.

Methodology: Baoqiang Li, Xuecong Lu, Mohammad Moeini, Sava Sakadžić.

Project administration: Frederic Lesage.

Resources: Frederic Lesage.

Software: Xuecong Lu, Mohammad Moeini.

Supervision: Eric Thorin, Frederic Lesage.

Validation: Mohammad Moeini, Sava Sakadžić.

Visualization: Baoqiang Li, Xuecong Lu.

Writing – original draft: Baoqiang Li.

Writing – review & editing: Baoqiang Li, Xuecong Lu, Mohammad Moeini, Sava Sakadžić, Eric Thorin, Frederic Lesage.

References

1. Kalback W, Esh C, Castaño EM, Rahman A, Kokjohn T, Luehrs DC, et al. Atherosclerosis, vascular amyloidosis and brain hypoperfusion in the pathogenesis of sporadic Alzheimer's disease. Neurol Res. 2004; 26: 525–539. https://doi.org/10.1179/016164104225017668 PMID: 15265270
2. de la Torre JC. Vascular risk factor detection and control may prevent Alzheimer's disease. Ageing Res Rev. 2010; 9: 218–225. https://doi.org/10.1016/j.arr.2010.04.002 PMID: 20385255
3. Iadecola C. The overlap between neurodegenerative and vascular factors in the pathogenesis of dementia. Acta Neuropathol (Berl). 2010; 120: 287–296. https://doi.org/10.1007/s00401-010-0718-6 PMID: 20623294
4. Leenders KL, Perani D, Lammertsma AA, Heather JD, Buckingham P, Jones T, et al. CEREBRAL BLOOD FLOW, BLOOD VOLUME AND OXYGEN UTILIZATIONNORMAL VALUES AND EFFECT OF AGE. Brain. 1990; 113: 27–47. https://doi.org/10.1093/brain/113.1.27 PMID: 2302536
5. Moskowitz MA, Lo EH, Iadecola C. The Science of Stroke: Mechanisms in Search of Treatments. Neuron. 2010; 67: 181–198. https://doi.org/10.1016/j.neuron.2010.07.002 PMID: 20670828
6. Pantoni L. Cerebral small vessel disease: from pathogenesis and clinical characteristics to therapeutic challenges. Lancet Neurol. 2010; 9: 689–701. https://doi.org/10.1016/S1474-4422(10)70104-6 PMID: 20610345
7. Chambless LE, Folsom AR, Clegg LX, Sharrett AR, Shahar E, Nieto FJ, et al. Carotid Wall Thickness is Predictive of Incident Clinical Stroke: The Atherosclerosis Risk in Communities (ARIC) Study. Am J Epidemiol. 2000; 151: 478–487. https://doi.org/10.1093/oxfordjournals.aje.a010233 PMID: 10707916
8. Ohira T, Shahar E, Chambless LE, Rosamond WD, Mosley TH, Folsom AR. Risk Factors for Ischemic Stroke Subtypes: The Atherosclerosis Risk in Communities Study. Stroke. 2006; 37: 2493–2498. https://doi.org/10.1161/01.STR.0000239694.19359.88 PMID: 16931783
9. Atherosclerotic Disease of the Aortic Arch as a Risk Factor for Recurrent Ischemic Stroke. N Engl J Med. 1996; 334: 1216–1221. https://doi.org/10.1056/NEJM199605093341902 PMID: 8606716
10. Kivipelto M, Helkala E-L, Laakso MP, Hänninen T, Hallikainen M, Alhainen K, et al. Midlife vascular risk factors and Alzheimer's disease in later life: longitudinal, population based study. BMJ. 2001; 322: 1447–1451. https://doi.org/10.1136/bmj.322.7300.1447 PMID: 11408299
11. Jurado M-B, Palacios M, Moreno-Zambrano D, Cevallos C, Regato I, Gamboa X, et al. Cardiovascular risk factors contribute differentially to cognitive functioning in middle-aged adults (P6.323). Neurology. 2017; 88: P6.323.

12. Hofman A, Ott A, Breteler MM, Bots ML, Slooter AJ, van Harskamp F, et al. Atherosclerosis, apolipoprotein E, and prevalence of dementia and Alzheimer's disease in the Rotterdam Study. The Lancet. 1997; 349: 151–154. https://doi.org/10.1016/S0140-6736(96)09328-2

13. Dickstein DL, Walsh J, Brautigam H, Stockton SD, Gandy S, Hof PR. Role of Vascular Risk Factors and Vascular Dysfunction in Alzheimer's Disease. Mt Sinai J Med J Transl Pers Med. 77: 82–102. https://doi.org/10.1002/msj.20155 PMID: 20101718

14. Yaffe K, Vittinghoff E, Pletcher MJ, Hoang T, Launer L, Whitmer R, et al. Early Adult to Mid-Life Cardiovascular Risk Factors and Cognitive Function. Circulation. 2014; CIRCULATIONAHA.113.004798. https://doi.org/10.1161/CIRCULATIONAHA.113.004798 PMID: 24687777

15. Popa-Wagner A, Buga A-M, Popescu B, Muresanu D. Vascular cognitive impairment, dementia, aging and energy demand. A vicious cycle. J Neural Transm Vienna Austria 1996. 2015; 122 Suppl 1: S47–54. https://doi.org/10.1007/s00702-013-1129-3 PMID: 24337666

16. Peers C, Dallas ML, Boycott HE, Scragg JL, Pearson HA, Boyle JP. Hypoxia and Neurodegeneration. Ann N Y Acad Sci. 1177: 169–177. https://doi.org/10.1111/j.1749-6632.2009.05026.x PMID: 19845619

17. Peers C, Pearson HA, Boyle JP. Hypoxia and Alzheimer's disease. Essays Biochem. 2007; 43: 153–164. https://doi.org/10.1042/BSE0430153 PMID: 17705799

18. Guyton AC. Textbook of medical physiology. 1981; Available: http://agris.fao.org/agris-search/search.do?recordID=XF2015006074

19. Jespersen SN, Østergaard L. The roles of cerebral blood flow, capillary transit time heterogeneity, and oxygen tension in brain oxygenation and metabolism. J Cereb Blood Flow Metab. 2012; 32: 264–277. https://doi.org/10.1038/jcbfm.2011.153 PMID: 22044867

20. Østergaard L, Engedal TS, Aamand R, Mikkelsen R, Iversen NK, Anzabi M, et al. Capillary transit time heterogeneity and flow-metabolism coupling after traumatic brain injury. J Cereb Blood Flow Metab. 2014; 34: 1585–1598. https://doi.org/10.1038/jcbfm.2014.131 PMID: 25052556

21. Eskildsen SF, Gyldensted L, Nagenthiraja K, Nielsen RB, Hansen MB, Dalby RB, et al. Increased cortical capillary transit time heterogeneity in Alzheimer's disease: a DSC-MRI perfusion study. Neurobiol Aging. 2017; 50: 107–118. https://doi.org/10.1016/j.neurobiolaging.2016.11.004 PMID: 27951412

22. Finikova OS, Lebedev AY, Aprelev A, Troxler T, Gao F, Garnacho C, et al. Oxygen Microscopy by Two-Photon-Excited Phosphorescence. ChemPhysChem. 2008; 9: 1673–1679. https://doi.org/10.1002/cphc.200800296 PMID: 18663708

23. Sakadžić S, Roussakis E, Yaseen MA, Mandeville ET, Srinivasan VJ, Arai K, et al. Two-photon high-resolution measurement of partial pressure of oxygen in cerebral vasculature and tissue. Nat Methods. 2010; 7: 755–759. https://doi.org/10.1038/nmeth.1490 PMID: 20693997

24. Lecoq J, Parpaleix A, Roussakis E, Ducros M, Houssen YG, Vinogradov SA, et al. Simultaneous two-photon imaging of oxygen and blood flow in deep cerebral vessels. Nat Med. 2011; 17: 893–898. https://doi.org/10.1038/nm.2394 PMID: 21642977

25. Sanan DA, Newland DL, Tao R, Marcovina S, Wang J, Mooser V, et al. Low density lipoprotein receptor-negative mice expressing human apolipoprotein B-100 develop complex atherosclerotic lesions on a chow diet: no accentuation by apolipoprotein(a). Proc Natl Acad Sci U S A. 1998; 95: 4544–4549. 10.1073/pnas.95.8.4544 PMID: 9539774

26. Li B, Maafi F, Berti R, Pouliot P, Rhéaume E, Tardif J-C, et al. Hybrid FMT-MRI applied to in vivo atherosclerosis imaging. Biomed Opt Express. 2014; 5: 1664–1676. https://doi.org/10.1364/BOE.5.001664 PMID: 24877023

27. Bolduc V, Drouin A, Gillis M-A, Duquette N, Thorin-Trescases N, Frayne-Robillard I, et al. Heart rate-associated mechanical stress impairs carotid but not cerebral artery compliance in dyslipidemic atherosclerotic mice. Am J Physiol Heart Circ Physiol. 2011; 301: H2081–H2092. https://doi.org/10.1152/ajpheart.00706.2011 PMID: 21926346

28. Drouin A, Bolduc V, Thorin-Trescases N, Bélanger É, Fernandes P, Baraghis E, et al. Catechin treatment improves cerebrovascular flow-mediated dilation and learning abilities in atherosclerotic mice. Am J Physiol—Heart Circ Physiol. 2011; 300: H1032–H1043. https://doi.org/10.1152/ajpheart.00410.2010 PMID: 21186270

29. Moeini M, Lu X, Avti PK, Damseh R, Bélanger S, Picard F, et al. Compromised microvascular oxygen delivery increases brain tissue vulnerability with age. Sci Rep. 2018; 8: 8219. https://doi.org/10.1038/s41598-018-26543-w PMID: 29844478

30. Lu X, Li B, Moeini M, Lesage F. Simultaneous two-photon imaging of cerebral oxygenation and capillary blood flow in atherosclerotic mice. 2017. pp. 100510O–100510O–6. https://doi.org/10.1117/12.2251437

31. Bolduc V, Baraghis E, Duquette N, Thorin-Trescases N, Lambert J, Lesage F, et al. Catechin prevents severe dyslipidemia-associated changes in wall biomechanics of cerebral arteries in LDLr-/-:hApoB+/+ mice and improves cerebral blood flow. Am J Physiol Heart Circ Physiol. 2012; 302: H1330–9. https://doi.org/10.1152/ajpheart.01044.2011 PMID: 22268108

32. Drouin A, Farhat N, Bolduc V, Thorin-Trescases N, Gillis MA, Villeneuve L, et al. Up-regulation of thromboxane A_2 impairs cerebrovascular eNOS function in aging atherosclerotic mice. Pflugers Arch. 2011; 462: 371–383. https://doi.org/10.1007/s00424-011-0973-y PMID: 21617900

33. Farhat N, Thorin-Trescases N, Mamarbachi M, Villeneuve L, Yu C, Martel C, et al. Angiopoietin-like 2 promotes atherogenesis in mice. J Am Heart Assoc. 2013; 2: e000201. https://doi.org/10.1161/JAHA.113.000201 PMID: 23666461

34. Gendron M-È, Théorêt J-F, Mamarbachi AM, Drouin A, Nguyen A, Bolduc V, et al. Late chronic catechin antioxidant treatment is deleterious to the endothelial function in aging mice with established atherosclerosis. Am J Physiol Heart Circ Physiol. 2010; 298: H2062–H2070. https://doi.org/10.1152/ajpheart.00532.2009 PMID: 20382853

35. Nguyen A, Duquette N, Mamarbachi M, Thorin E. Epigenetic Regulatory Effect of Exercise on Glutathione Peroxidase 1 Expression in the Skeletal Muscle of Severely Dyslipidemic Mice. PloS One. 2016; 11: e0151526. https://doi.org/10.1371/journal.pone.0151526 PMID: 27010651

36. Santisakultarm TP, Cornelius NR, Nishimura N, Schafer AI, Silver RT, Doerschuk PC, et al. In vivo two-photon excited fluorescence microscopy reveals cardiac- and respiration-dependent pulsatile blood flow in cortical blood vessels in mice. Am J Physiol Heart Circ Physiol. 2012; 302: H1367–1377. https://doi.org/10.1152/ajpheart.00417.2011 PMID: 22268102

37. Kleinfeld D, Mitra PP, Helmchen F, Denk W. Fluctuations and stimulus-induced changes in blood flow observed in individual capillaries in layers 2 through 4 of rat neocortex. Proc Natl Acad Sci. 1998; 95: 15741–15746. https://doi.org/10.1073/pnas.95.26.15741 PMID: 9861040

38. Li B, Wang H, Fu B, Wang R, Sakadžić S, Boas DA. Impact of temporal resolution on estimating capillary RBC-flux with optical coherence tomography. J Biomed Opt. 2017; 22: 016014–016014. https://doi.org/10.1117/1.JBO.22.1.016014 PMID: 28125157

39. Golub AS, Pittman RN. Erythrocyte-associated transients in PO2 revealed in capillaries of rat mesentery. Am J Physiol Heart Circ Physiol. 2005; 288: H2735–2743. https://doi.org/10.1152/ajpheart.00711.2004 PMID: 15695557

40. Mintun MA, Lundstrom BN, Snyder AZ, Vlassenko AG, Shulman GL, Raichle ME. Blood flow and oxygen delivery to human brain during functional activity: Theoretical modeling and experimental data. Proc Natl Acad Sci. 2001; 98: 6859–6864. https://doi.org/10.1073/pnas.111164398 PMID: 11381119

41. Sakadžić S, Mandeville ET, Gagnon L, Musacchia JJ, Yaseen MA, Yucel MA, et al. Large arteriolar component of oxygen delivery implies a safe margin of oxygen supply to cerebral tissue. Nat Commun. 2014; 5. https://doi.org/10.1038/ncomms6734 PMID: 25483924

42. Parpaleix A, Houssen YG, Charpak S. Imaging local neuronal activity by monitoring PO2 transients in capillaries. Nat Med. 2013; 19: 241–246. https://doi.org/10.1038/nm.3059 PMID: 23314058

43. Lyons DG, Parpaleix A, Roche M, Charpak S. Mapping oxygen concentration in the awake mouse brain. eLife. 2016; 5: e12024. https://doi.org/10.7554/eLife.12024 PMID: 26836304

44. Desjardins M, Berti R, Lefebvre J, Dubeau S, Lesage F. Aging-related differences in cerebral capillary blood flow in anesthetized rats. Neurobiol Aging. 2014; 35: 1947–1955. https://doi.org/10.1016/j.neurobiolaging.2014.01.136 PMID: 24612672

45. VanTeeffelen JWGE, Constantinescu AA, Brands J, Spaan JAE, Vink H. Bradykinin- and sodium nitroprusside-induced increases in capillary tube haematocrit in mouse cremaster muscle are associated with impaired glycocalyx barrier properties. J Physiol. 586: 3207–3218. https://doi.org/10.1113/jphysiol.2008.152975 PMID: 18450777

46. Celermajer DS, Sorensen KE, Gooch VM, Spiegelhalter DJ, Miller OI, Sullivan ID, et al. Non-invasive detection of endothelial dysfunction in children and adults at risk of atherosclerosis. The Lancet. 1992; 340: 1111–1115. https://doi.org/10.1016/0140-6736(92)93147-F

47. Davignon J, Ganz P. Role of endothelial dysfunction in atherosclerosis. Circulation. 2004;109: III27-32. https://doi.org/10.1161/01.CIR.0000137284.17083.93

48. Tomita Y, Tomita M, Schiszler I, Amano T, Tanahashi N, Kobari M, et al. Moment analysis of microflow histogram in focal ischemic lesion to evaluate microvascular derangement after small pial arterial occlusion in rats. J Cereb Blood Flow Metab Off J Int Soc Cereb Blood Flow Metab. 2002; 22: 663–669. https://doi.org/10.1097/00004647-200206000-00004 PMID: 12045664

49. Pries AR, Secomb TW, Gaehtgens P. Biophysical aspects of blood flow in the microvasculature. Cardiovasc Res. 1996; 32: 654–667. PMID: 8915184

50. Janssen BJA, De Celle T, Debets JJM, Brouns AE, Callahan MF, Smith TL. Effects of anesthetics on systemic hemodynamics in mice. Am J Physiol-Heart Circ Physiol. 2004; 287: H1618–H1624. https://doi.org/10.1152/ajpheart.01192.2003 PMID: 15155266